Investigating Atmospheric Ice Crystal Formation and Their Impacts on Hypersonic Vehicles

Imteaz Osmani*, Victor Ojo†, Lance Roadifer‡, Christian Nairy§, Aaron Kennedy¶, David Delene‖ and Hallie Chelmo**
University of North Dakota, Grand Forks, ND, 58202, USA

Siddharth Bhatnagar††, Yidi Gao‡‡, Joseph J. Lavalley§§, Matthieu Shelby ¶¶, Eleanor C. Hostetler***, Matthew S. Leight††† and Joseph S. Jewell‡‡‡
Purdue University, West Lafayette, IN, 47907, USA

In the atmosphere, the formation of ice crystal chains, or aggregates, occurs when micrometer-sized atmospheric ice particles stick together, as observed in situ during recent aircraft campaigns. Atmospheric ice exists at various altitudes and latitudes, including polar and tropical regions, and poses a potential threat to hypersonic vehicles (re-entry vehicles, missiles, or jet aircrafts) due to the risk of impact. In this work, the impact of hypersonic speeds on atmospherically realistically sized ice particles is examined by generating them under controlled laboratory conditions, with the aim of introducing them into high-speed flow facilities and recording their interactions. The Purdue 3-inch shock tube is used here. At the University of North Dakota, techniques been developed for forming and stably suspending ice crystals and ice crystal aggregates. Images of these laboratory-grown ice particles are presented here. Replicating the formation of ice crystals and their aggregates in realistic atmospheric conditions is challenging in laboratory settings because of their delicate nature. It therefore requires a novel approach that allows microdroplet freezing without physical contact, which could alter the freezing mechanisms and the resulting ice morphology. To achieve this, two microparticle levitation techniques are used at temperatures below 0°C: an acoustic levitator and an electrodynamic balance. The acoustic levitator generates standing ultrasonic sound waves, resulting in a vertical stack of minimum pressure points, trapping droplets within these minima by balancing gravity with acoustic forces. Furthermore, efforts to dispense the acoustically levitated ice crystals directly into Purdue's 3-inch shock tube are discussed. Ultimately, understanding how shock waves interact with ice crystals will improve efforts in minimizing potential damage to hypersonic vehicles. The electrodynamic balance, which traps charged droplets in the size range of tens of micrometers, currently operates with temperatures down to -5.4°C. This enables the freezing of water droplets containing ice nucleating particles. Addtionally, there are two balances located in this electrodynamic balance, which makes it possible to create on-demand ice crystal aggregates found in atmospheric clouds.

*Graduate Research Assistant, Department of Mechanical Engineering. imteaz.osmani@und.edu
†Graduate Research Assistant, Department of Mechanical Engineering. victor.ojo@und.edu
‡Undergraduate Research Assistant, Department of Mechanical Engineering. lance.roadifer@und.edu
§Graduate Research Assistant, Department of Atmospheric Sciences. christian.nairy@und.edu
¶Associate Professor, Department of Atmospheric Science. aaron.kennedy@und.edu
‖Research Professor, Department of Atmospheric Science. david.delene@und.edu
**Assistant Professor, Department of Mechanical Engineering. hallie.chelmo@und.edu
††Graduate Research Assistant, School of Aeronautics and Astronautics, AIAA Student Member. bhatna11@purdue.edu
‡‡Graduate Research Assistant, School of Aeronautics and Astronautics, AIAA Student Member. gao696@purdue.edu
§§Graduate Research Assistant, School of Aeronautics and Astronautics, AIAA Student Member. jlavall@purdue.edu
¶¶Undergraduate Research Assistant, School of Aeronautics and Astronautics. matthieushelby68@gmail.com
***Undergraduate Research Assistant, School of Aeronautics and Astronautics. hostetl9@purdue.edu
†††Undergraduate Research Assistant, School of Aeronautics and Astronautics. leight@purdue.edu
‡‡‡John Bogdanoff Associate Professor, School of Aeronautics and Astronautics, AIAA Associate Fellow. jsjewell@purdue.edu

I. Nomenclature

DBET	=	Dual Balance Electrostatic Trap
PHIPS	=	Particle Habit Imaging and Polar Scattering
P3IST	=	Purdue 3-Inch Shock Tube
IMPACTS	=	Investigation of Microphysics and Precipitation for Atlantic Coast-Threatening
*CapeEx*19	=	Cape Canaveral Experiment in 2019
CPI	=	Cloud Particle Imaging
INP	=	Ice Nucleating Particle

II. Background

ELONGATED,chain-like ice crystal and frozen droplet aggregates have been observed (in situ) in both summertime, convection-induced cirrus anvils, and in the mid-to-upper-level clouds of wintertime snowstorms (Figure 1). Chain-like ice crystals have also been generated in cloud chamber experiments using high electric fields and ice crystal concentrations at various sub-freezing temperatures[1]. While electric fields act to enhance chain aggregation, details of the location(s) where the chain aggregation process occurs in clouds are not well understood; therefore, the chain aggregation process cannot be incorporated into atmospheric cloud models. Since chain aggregates are unique and contain various quantities of individual ice particles and/or frozen droplets, they have more mass and different radiative scattering properties than individual ice crystals. Without accounting for chain aggregates in radiative transfer models results in inaccurate radiative scatter properties of clouds[2]. Moreover, without accounting for chain aggregate particles in atmospheric cloud models causes uncertainties when modeling supersonic projectile trajectories that intersect cirrus cloud anvils [3]. The uncertainties are due to hypersonic collisions with relatively large, chain-like ice crystals, which can cause cratering on the vehicle's nose cone [4], altering the vehicle's aerodynamics [5] [6] [7].

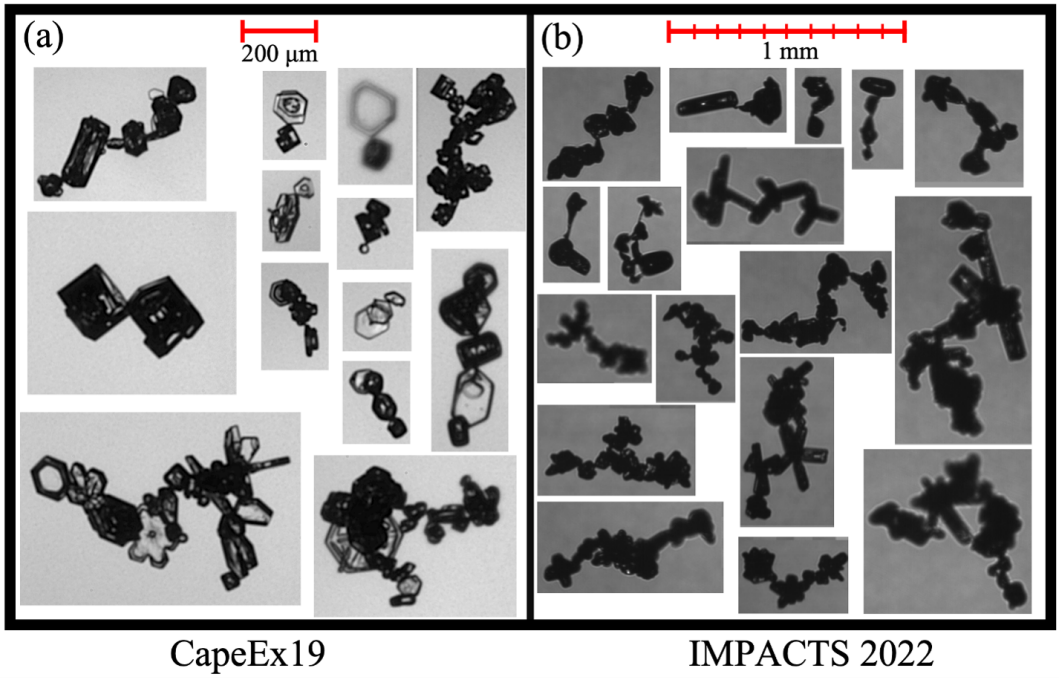

Fig. 1 Collage of chain aggregates (a) imaged by the Particle Habit Imaging and Polar Scattering (PHIPS) probe during the Cape Canaveral Experiment in 2019 (CapeEx19) and (b) imaged by the Hawkeye-Cloud Particle Imaging (CPI) probe during the Investigation of Microphysics and Precipitation for Atlantic Coast-Threatening Snowstorms (IMPACTS) field campaign in 2022. Acknowledgments for the PHIPS images: Emma Järvinen and Martin Schnaiter from Karlsruhe Institute of Technology (KIT).

This work presents aircraft observations of chain-like ice aggregates collected in recent CapeEx19 and laboratory methods to enhance our understanding of their formation and their interactions with shock waves. The high-resolution capabilities of the PHIPS probe [8] clearly illustrated small joints bridging multiple crystal elements (Figure 1) [9]. Therefore, to generate and study the ice crystals in a laboratory, two approaches are taken. The first one is the acoustic levitator which uses ultrasonic sound waves (approximately 40KHz) to levitate ice crystals. This acoustic levitator will be integrated with the shock tube to study the hypersonic influence in the presence of ice crystals. As demonstrated in this work, ice crystals are generated inside the acoustic levitator by freezing suspended water droplets, as well as vapor deposition ice crystal formation. The acoustically levitated ice crystal sizes and shapes will be characterized and introduced into the shock tube in the path of the shockwave. Using a high-speed camera, the interaction of shockwaves and ice crystals will be recorded to measure their thermodynamic and mechanical changes, such as melting, cracking, and sublimation. The second device is a novel instrument that produces and traps two micrometer-sized droplets without any physical contact. It is outfitted with a custom built cooling system to achieve freezing temperatures for generating and levitating ice crystal aggregates inside the instrument.

III. Acoustically levitated ice crystals

An acoustic levitator is used in this work to levitate liquid water droplets ranging in sizes from hundreds of micrometers to a few millimeters, and subsequently freeze them to create ice crystals. The mechanism for trapping and levitating the droplets is described in previous literature [10]. Briefly, the setup contains an array of transducers and reflectors arranged to generate high-frequency (ultrasonic) sound waves reflect and resonate, producing low and high-pressure and standing waves in the middle. These standing nodes have multiple nodes and anti-nodes at specific intervals. The nodes and antinodes are the maximum and minimum pressure points, respectively. Droplets are trapped at the minimum pressure point where gravity and acoustic pressure are balanced. After generating the acoustically levitated ice crystals, they can be introduced into Purdue's 3-inch shock tube to measure their responses to shock waves at varying Mach values.

The acoustic levitator is a commercially available instrument, TinyLev [10]. The TinyLev enables homogenous freezing, which occurs when water droplets freeze without contact with any ice nucleants. Pure water homogenous freezing has been observed at or below -36°C [11][12][13]. In contrast, heterogeneous freezing occurs at much warmer temperatures reportedly between 0 to -36 °C [14], [15]. This indicates that atmospheric microdroplets may freeze in through a variety of mechanisms that depend on the absence or presence of ice-nucleating particles [12], [15], [16].

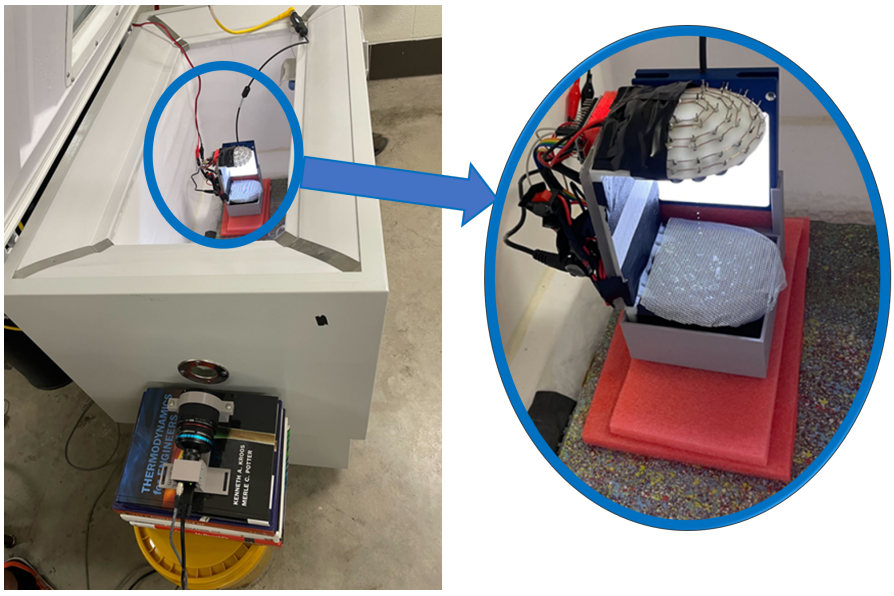

Fig. 2 The above image shows a ScienTemp chest freezer setup used for imaging acoustically suspended ice crystals. The blue circled section shows the close-up of the acoustic levitator in the freezer placed on a custom 3D printed base and paddings. The illuminated backlight is the strobe LED backlight which is paired with a FLIR USB-3 camera.

Two cooling methods are employed for generating ice crystals in an acoustic levitator. In the first method, the acoustic levitator was placed inside a ScienTemp chest freezer, as shown in Figure 2. The chest freezer is set to -40°C. Inside the acoustic levitator two temperature probes were attached. The first temperature probe was placed in the middle of the levitator, a few inches from the droplet, that read approximately -27°C. The second temperature probe was placed near the bottom plate to cross check with the first temperature probe. This large difference is due to the chest freezer's top lid being open for most of the the experiment. The droplets are dispensed inside the acoustic levitator for trapping by using two methods: micropipettes and a mist fan. For the micropipette dispending method, droplet volumes between 3-8 µL are loaded at the minimum pressure nodes. The droplet volumes from the mist fan are smaller, but not measured. Droplets are loaded while the acoustic levitator is secured inside the freezer.

Freezing the suspended droplets is observed as they thermally equilibrate with the freezer air. Different shapes of ice crystals are produced in the trap, such as disks, plates, and irregular shapes. To image these resulting structures, a backlit version of the Open Snowflake Camera for Research and Education (OSCRE) is used to capture different ice crystal shapes [17]. A Teledyne/FLIR 3.2MP USB-3 machine vision camera is paired to a strobed LED backlight. The camera and 85mm lens is installed through a chest freezer inlet port, and the acoustic levitator is placed inside the freezer on a custom 3D-printed base with the LED strobe light. Frames per second of each video are noted and the length of each pixel of the camera is 10 µm. Freezing times are calculated by counting the frame numbers in each frames/second and ice crystal sizes are measured with MATLAB image processing [18]. The camera and the flash operate in command mode for the entire image-capturing session with a varying frame rate from 30 frames/second to 120 frames/second.

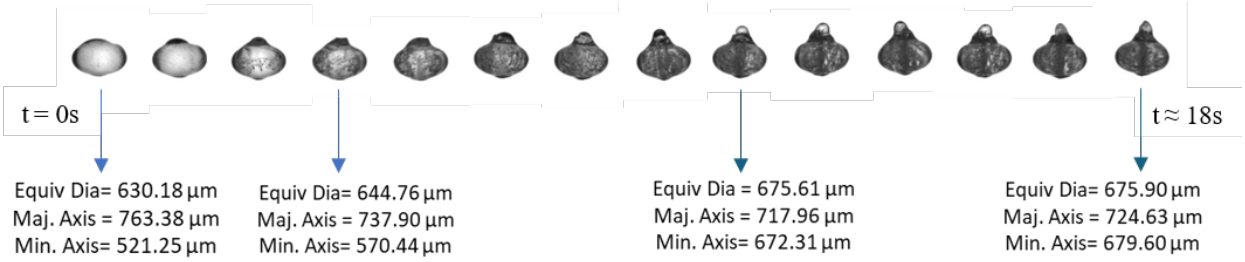

Fig. 3 Time series of an acoustically levitated water microdroplet undergoing freezing (from left to right) resulting in a non-spherical shape, recorded using OSCRE with a total time of approximately 18 seconds. Here, t = 0 is the time when droplet was dispensed in the acoustic levitator and immediately begins to freeze from the surface. On the right side, t ≈ 18 s denotes the approximate time when the droplet is completely frozen. Ice particles such as this can be introduced into high-speed flow facilities in order to observe their changes when interacting with a shock wave.

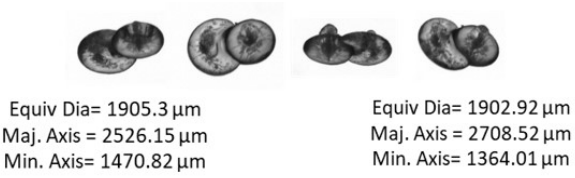

Fig. 4 A single acoustically levitated ice crystal aggregate, or two joined ice particles, formed by dispensing a liquid micrdroplet onto an already suspended frozen droplet. The aggregate's rotational motion enables multiple angles to observe the full three dimensional structure. The images are taken using OSCRE. If impacted by a shock wave, an aggregate such as this one would either break apart or remain stuck together.

Inside the chest freezer, another type of heterogeneous freezing called deposition freezing is observed[19],[20],[21]. Deposition freezing occurs when there is supersaturation with respect to ice and the temperature is below 0 °C. Water vapor condenses directly onto an ice-nucleating particle, creating an ice crystal. In the acoustic levitation experiment, the mist creates this supersaturation, allowing water vapor to deposit on a ice nucleating particle coincident with the low pressure nodes. The ice crystal grows freely in the supersaturated gaseous surroundings. The observed shapes include plate and disk-type ice crystals, as shown in Figure 5. Previous work asserted that columnar and dendritic ice crystals

have been observed below -19 °C and -34.7 °C, which is near the homogeneous temperature [22]. In a shockwave environment, different ice crystal shapes can respond differently, but there is a lack of data to test this question.

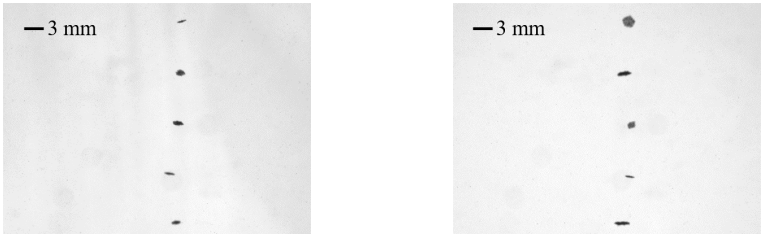

(a) Disc shapes formed from deposition freezing (Frame number 268). **(b) Disc shapes formed from deposition freezing (Frame number 908).**

Fig. 5 Two differnet angles of the same vertical stack of ice crystals spontaneously formed from deposition freezing inside the chest freezer. The videos of deposition freezing are available in Supplemental Information.

The acoustically levitated ice crystals formed inside the chest freezer are useful for high resolution images captured with OSCRE, as in (Figure 3-4). However, to study shock wave and ice crystal interactions, it is necessary to generate ice crystals in the acoustic levitator without the help of a chest freezer, as the chest freezer cannot be integrated with a high speed flow platform. Therefore, ice crystals are also generated independently, allowing the acoustic levitator to be integrated with a shock tube port. This enables the introduction of ice crystals to the shockwave path. A recent study[23] uses a "cryogun" technique for freezing acoustically levitated droplets with a metal container allowing a cold stream to flow over the suspended droplets via natural convection when the container is filled with liquid N_2. In this work, a similiar concept is demonstrated, where a volumetric flask filled with liquid N_2 guides the cold air stream through a plastic funnel fastened to the top of the acoustic levitator. This "cryo-beaker" approach successfully demonstrates ice crystal formation in the trap without the large chest freezer. Figure 6-7 shows various crystal forms generated using this setup. These images are captured with a Raspberry Pi HQ camera. With ice crystal formation possible using an acoustic levitator, this setup is now ready to be united with a port of Purdue's 3-inch shock tube (P3IST), through which generated ice crystals can be dropped inside the shock tube. To accomplish this step, several design challenges will be addressed in upcoming work.

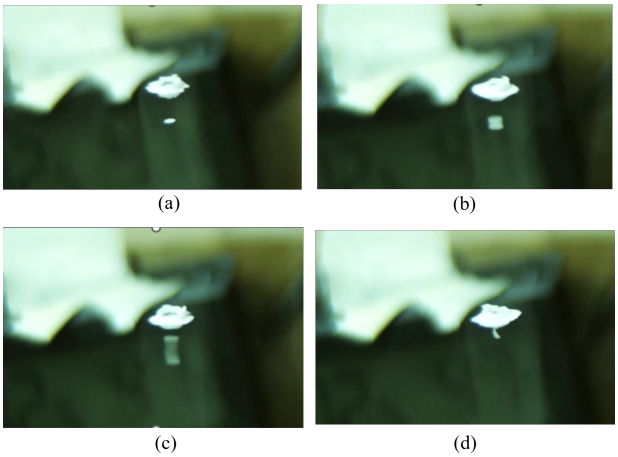

Fig. 6 Images showing an acoustically levitated ice crystal aggregating with a larger ice crystal above it. The vertical translucent region around the droplet is the cold air stream due to liquid N_2 in the cryo beaker.

From visual inspection using a borescope camera, it is evident that the droplets oscillate in the levitator at specific nodal locations. One experiment using an SA4 highspeed camera at 5000 fps and a continuous light source measures the oscillation of liquid droplets in the acoustic levitator. Droplets in the levitator are visibly flattened and deformed into ellipsoids, a result of the horizontal oscillations and vertical compression from standing waves. Oscillation frequency in

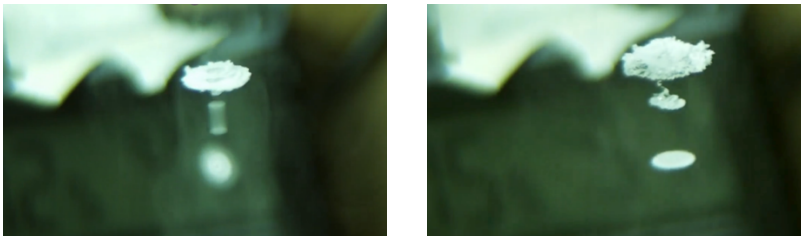

(a) Images showing multiple acoustically levitated ice crystals. There are three different crystal formations. From top to bottom, there is a frozen spherical droplet exhibiting riming; the middle is a column; the bottom is a flat discshape.This illustrates the variety of ice crystals formed during one experiment. All of these ice crystals were oscillating and rotating at higher rpm.

(b) Cloud-shaped ice crystal with a tail which disintegrated later due to oscillation and rotation motion. A flat plate type droplet was also formed at the bottom.

Fig. 7 Different ice crystal shapes observed in the acoustic levitator through Raspberry Pi HQ camera.

the horizontal direction is plotted in Figure 8. There are relatively minor oscillations present in the vertical direction as well, which have not been analyzed.

Droplets' oscillation frequencies shown in Figure 8, comprised of 16-time segments from 5 high-speed imaging trials, with square icons representing the mean frequency for each droplet size. Smaller (4 µL) droplets oscillate at a higher frequency range than larger (5 µL); however, both cases remain in the low frequency range between 7 and 13 Hz.

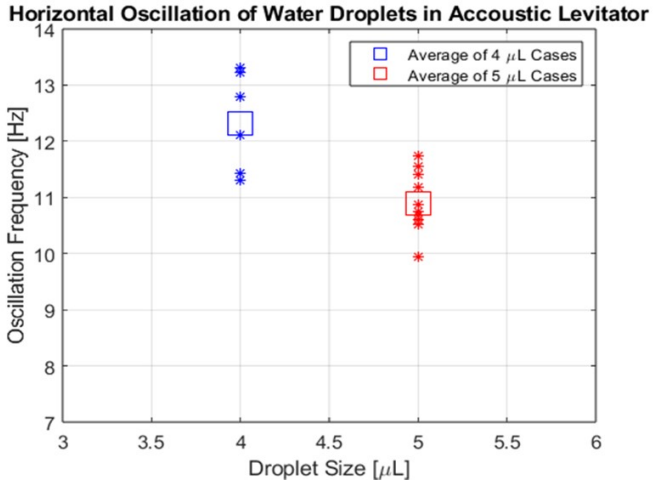

Fig. 8 Change of oscillation frequency with the change of water droplet volume.

This work presents a reliable and repeatable technique for producing acoustically levitated ice crystals that can be applied to shock tube experiments. For integrating the levitator into a shock tube port, the acoustic levitator needs to be placed on top of a platform attached on top of the acoustic levitator. In the place Pico-pulse droplet dispenser (Figure 11), it will be placed. For dropping ice crystals, the port needs to be opened and closed in fractions of seconds to drop the ice crystal into the shock tube and not re-pressurize the lower pressure-driven section at the same time.

The next steps with acoustic levitation will entail temperature and humidity sensors for measuring the gaseous conditions during freezing, for eventually. Also by incorporating a flow control mechanism into the cool air flow crystal growth can be controlled.

IV. Electrodynamically Levitated Ice Crystals

Towards replicating individual ice crystal aggregates, such as those observed in clouds shown in Figure 4, the electrodynamic balance utilized in this work uniquely traps multiple microparticles with the capability of merging ice crystals in two electrodynamic trapping regions. Electrodynamic balances have been utilized in atmospheric chemistry for several decades[24] [25] [26] [27] [28] [29] [30] and investigating microdroplet chemical reactions [31] [32] [33]. This Dual Balance Electrodynamic Trap (DBET), commercially procured from MicroLev, LLC, is explained in detail in a prior publication that specifically focuses on merging viscous droplets to measure their rheological properties [34]. A schematic for the DBET is shown in Figure 9. As shown, there are two trapping regions, a top balance region and a bottom balance region. The DBET traps aerosol particles axially through the electrodynamic field generated by the quadrupole electrodes and guides the particle to fall vertically by the counterbalance electrodes. The droplets are loaded in the trap by injection from a MicroFab droplet dispenser (MJ-ABP-01) with a 50 µm orifice. The droplet immediately gets charged via an induction electrode. Relative humidity (RH) inside the chamber is controlled by setting the fraction of the nitrogen flowing into a bubbler to add moisture to the flow; the higher the wet flow fraction, the higher the RH. For measuring the temperature and RH inside the chamber, a probe for each property is attached to the top balance. A Thorlabss DCC1645C-HQ CMOS camera captures droplet changes in shape in the bottom balance. In Figure 9a, liquid droplets are held in the trap, then in Figure 9b and in Figure 9c, they are frozen and merged together, respectively, resulting in an aggregate in the bottom balance. In the DBET, the levitated microdroplets range in sizes

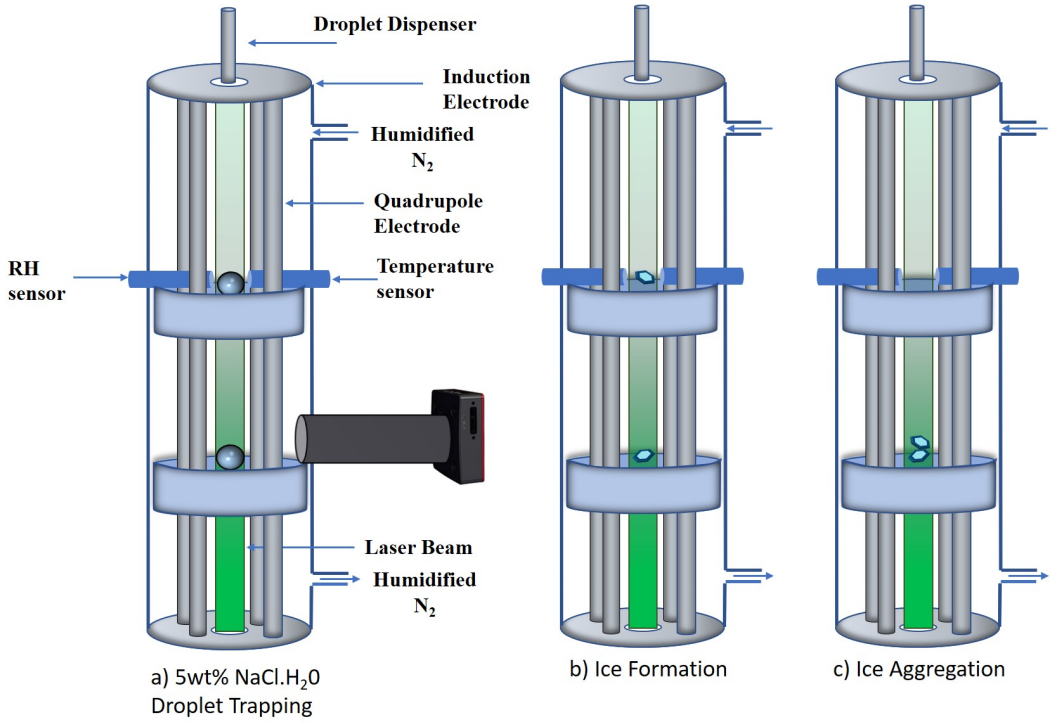

Fig. 9 Schematic Diagram of DBET (Dual Balance Electrodynamic trap). (a) Two oppositely charged water droplets are trapped in two balances. (b) Trapped water droplets are frozen down to ice crystals. (c) Aggregation of ice crystals and observation through a high-speed CMOS camera.

approximately 10 µm to 100 µm. When two droplets are loaded in the balance regions, they can be merged together to create one coalesced droplet for liquids or one aggregate for ice crystals. To produce an aggregate, temperature control at freezing temperatures is required. A custom designed copper tubing heat exchanger is attached to the DBET. Ice crystals are produced by freezing trapped water droplets. The chamber walls are cooled down gradually using a USA Labs UC-20/40 recirculating chiller that operates down to -40°C and uses propylene glycol and water at 60:40 ratio as a refrigerant. That refrigerant flows through the copper coil and the cooling line is also wrapped around with insulating material to minimize heat uptake from the surroundings. For minimizing condensation on the external equipment needed to operature the DBET, a plexiglass box encloses the setup and purges it with nitrogen gas.

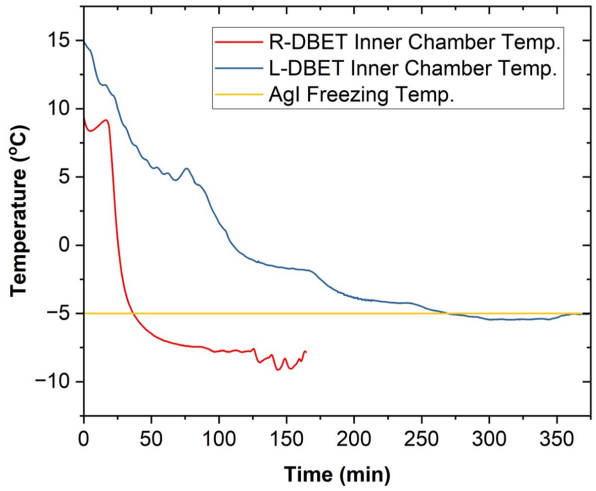

Fig. 10 The center line temperature (°C) inside the replica DBET (R-dBET) and the low temperature DBET (L-DBET) versus time (min.). The centerline temperature achieves a low enough temperature to heterogeneously freeze aqueous droplets containing silver iodide (AgI), a well-known and effective ice nucleating material. [35]

The temperature reduction in the DBET is essential for producing ice particles at atmospherically relevant sizes. The copper tubing was initially mounted on a replica of the geometry of the DBET's outer chamber, which does not contain any of the internal components. The main purpose of the replica is to be a mannequin; to ensure a tight fitting and maximize the contact with the real DBET. Figure 10 shows the measured centerline temperature reduction in the low temperature-DBET (L-DBET), as well as the replica (R-DBET). After approximately 160 minutes, the replica's center line temperature is -9°C. The low temperature-DBET only reaches -5.4°, which takes 300 minutes. The difference in efficiency is due to the low temperature-DBET interior, which is crowded instrument components. However, since the targeted water droplet chemical system is silver iodide (AgI), since AgI can initiate heterogeneous freezing at -5°C, although it can occur at temperatures up to -4°C [35] [36] [37].

The present work shows the low temperature DBET instrument is capable of producing complex ice crystal particulates, towards re-creating in situ observations from aircraft campaigns and advancing understanding of their formation and properties. This will be presented in upcoming work [38]. Additionally, ice crystal aggregation using the low temperature-DBET in Figure 9c can provide insight as to the conditions that promote their formation. Ultimately, more studies can be done on ice crystal chain formation and shockwave-ice crystal aggregate interaction.

V. Microdroplet Interactions with Shock Waves in the Purdue 3-inch Shock tube

The Purdue 3 Inch Shock Tube is used in this work to produce shock waves which can then hit water droplets and ice crystals. Interaction between the two can then be observed. Figure 11 below shows a schematic for the P3IST at Purdue ASL. The P3IST has an internal diameter of 3.5 inches (8.89cm), a driver-tube length of 1.43m, and a driven-tube length of 3.95m. Four sections of 304 stainless-steel pipe are machined together, ensuring matching of internal diameter throughout the tube [39], [40]. Pressure in the driven and driver sections is controlled by automated VAT Series 615 butterfly valves at both ends of the tube, designed to sustain a maximum differential pressure of 1 atm. An integrated PI controller controls the opening of the valve which allows both sections to track the designated pressure values within a quoted 0.05 percent error. The VAT valves have a 28000 increments position resolution from fully closed to fully open, with a complete closing/opening time of 0.6 seconds. Pre-run pressures in the driven section are measured by two Leybold CERAVAC CTR101 N active pressure sensors, with a quoted uncertainty of 0.12 percent for pressures above 0.13 bar. An analog signal between 0 and 10V is input directly into the VAT valve. These sensors are also capable of gas-independent pressure measurements by measuring changes in the capacitance of a diaphragm as it deforms. Pre-run pressures in the driver section are measured with a Paroscientific Model 745 Digiquartz® pressure transducer with a range of 0-15 psia (1034 mbar) and an accuracy of 0.008 percent. The transducer's digital output is converted to analog through a NI USB-6343 DAQ that operates at 500kS/s with 16-bit resolution [39]. A series of experiments were performed on the Purdue 3-Inch Shock Tube (P3IST) initially using natural bursting of the diaphragm

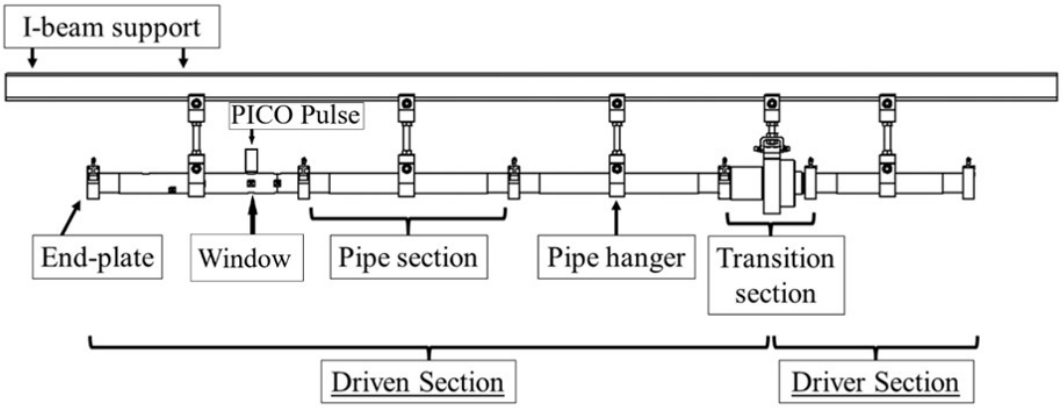

Fig. 11 P3IST Diagram [39] Adapted from Wason (2019)

by pressure difference alone. Later tests transitioned to controlled electrical bursts, using electrically heated wires to cut the diaphragm at a controlled pressure difference. Water droplets and droplets of water mixed with isopropyl alcohol, which had a lower surface tension than pure water, were dropped into the shock tube by use of a Nordson PICO Pulse dispenser. High-speed shadowgraphy and Schlieren images of shock-droplet interactions were recorded and aero-breakup of droplets were observed. Their respective breakup modes and mechanisms were identified and compared to expected breakup modes based on the Weber number. Images presented in this work were filmed based on a straight schlieren/shadowgraphy setup (Figure 12).

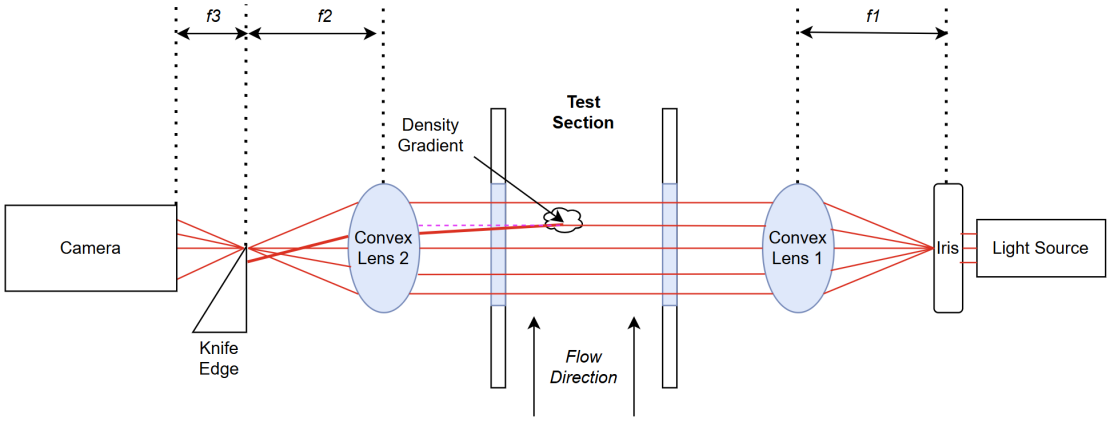

Fig. 12 Straight Schlieren/Shadowgraphy Setup Used for Images Presented in the Current Work

Droplet-shock interactions are classified into wave dynamics (Stage I) and droplet breakup dynamics (Stage II). Stage I concerns the interaction of an incident shock with the droplet surface leading to the creation of different wave structures like reflected wave, transmitted wave, Mach-stem, and diffracted wave, which affects the flow conditions around the droplet periphery. Droplets in Stage I experience deformation but retain their coherent structure, which is universal for all cases of shock-droplet interactions. Stage II describes the mechanism for the breakup and eventually disintegration of the droplet under these peripheral conditions [41]. Different modes are categorized by a non-dimensional quantity the Weber number, which is the ratio of the disturbing flow force and the stabilizing surface tension force, i.e. We= ρu2d/σ, where ρ is the gas density, u the freestream velocity, d the characteristic length and σ the surface tension force per unit surface area [42].

Previous work [42] listed 6 modes of droplet breakup: (1) vibrational breakup (8<We<12), (2) es breakup (12<We<50), (3) bag-and-stamen breakup (50<We<100), (4) sheet stripping (100<We<250), (5) wave crest stripping

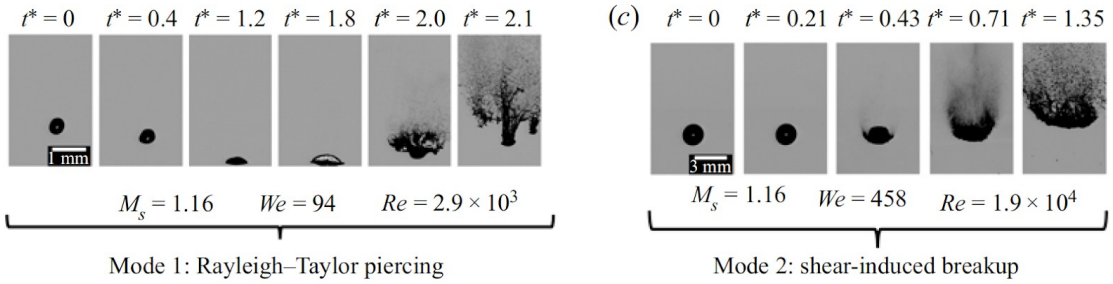

Fig. 13 Droplet breakup mechanisms (Stage II)[41].

(We>250) and (6) catastrophic breakup (We>250) [42]. The above 6 modes can be categorized into 2 groups shown below in (Figure 13) by their transition mechanisms: (1) Rayleigh-Taylor Piercing (RTP), and (2) Shear-Induced Entrainment (SIE). RTP breakups are induced by Rayleigh-Taylor instabilities on the droplet surface and SIE breakups are induced by the formation of Kelvin-Helmhotz waves on the surface.

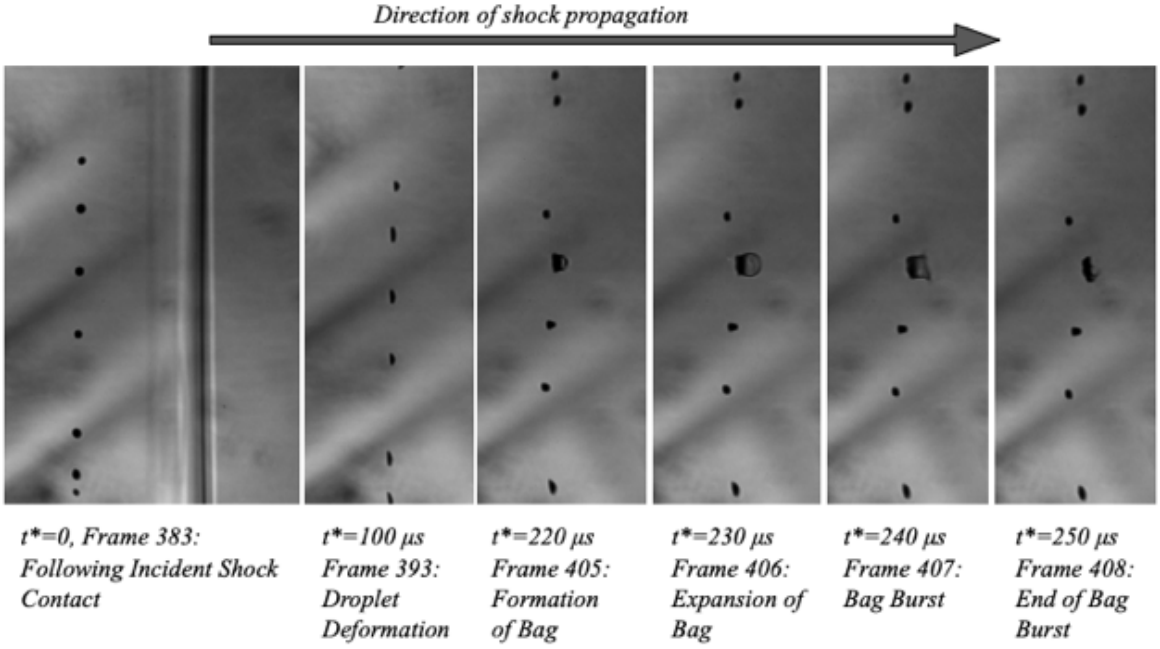

Fig. 14 : Electric Burst System Timing Tests, isolated time is the time it takes for the burst system to receive a start signal and burst the diaphragm, shock propagation time is the time it takes for the shock to travel from the diaphragm to the pressure sensor before the test section, and total time is the sum of these times.

Figure 14 shows the evolution of the droplet stream after the passage of an incident shock for one example test. Footage for this test was captured at 100000 fps with 1280 x 512 resolution using a Phantom TMX 7510. The initial pressure ratio of this burst was 2.2069 with an incident shock speed measured at 398.42 m/s and a contact surface propagation speed of 97.3158 m/s. Droplet sizes were estimated to be 0.25 mm, while the driven section density ρ is found via the equation of state to be 1.1899 kg/m3, while surface tension σ of water is 0.0728 N/m. The droplets were initially impacted by the flow induced by the incident shock and were visibly flattened into disc shapes. The bag formation was then observed in one of the droplets with an inflated water bubble which eventually burst, breaking up the droplet into several smaller droplets. Other droplets only experienced a brief deformation before returning to their original shapes due to the restoring forces of surface tension. The Weber number of the droplets was estimated to be 39. A bag-breakup was captured in 14. The above calculated Weber number falls in range of the bag-breakup mechanism which is a result of the Rayleigh-Taylor instability on the droplet surface. It was also evident that for a set Weber number,

droplets are not guaranteed to follow the prescribed mechanism and breakup, since only one among the entire droplet stream broke up while others retained integrity.

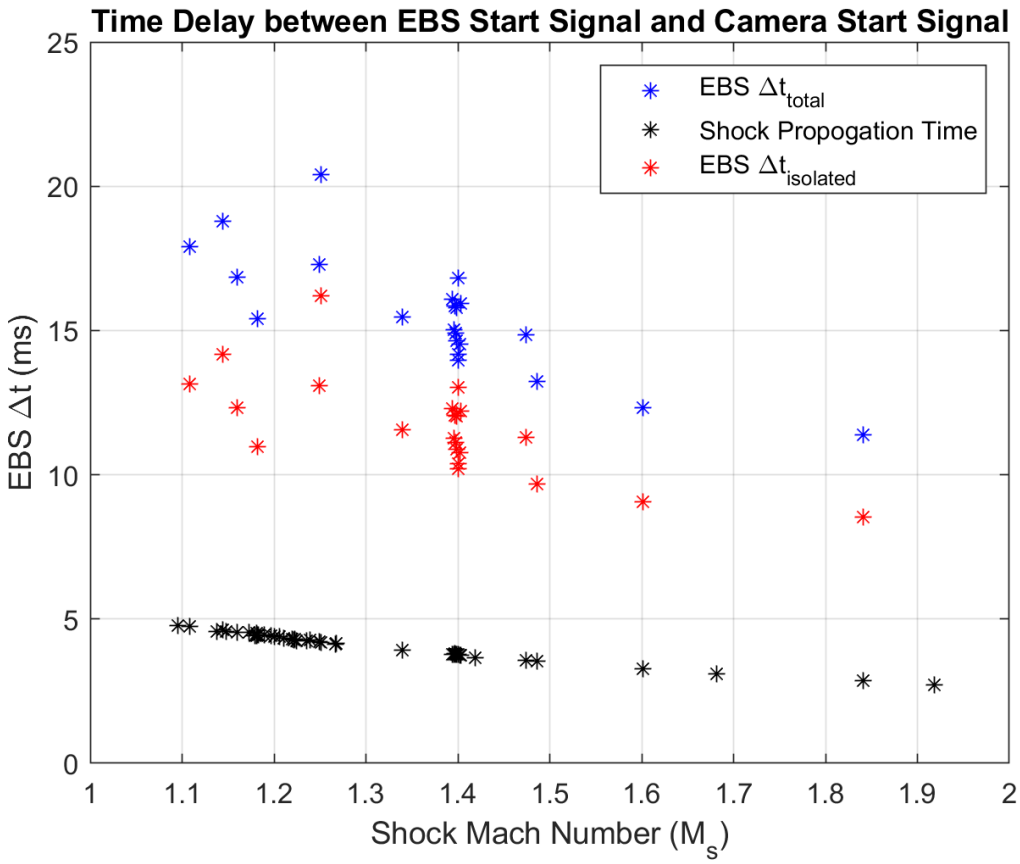

Fig. 15 : Electric Burst System Timing Tests, isolated time is the time it takes for the burst system to receive a start signal and burst the diaphragm, shock propagation time is the time it takes for the shock to travel from the diaphragm to the pressure sensor before the test section, and total time is the sum of these times.

Various tests were conducted and plotted according to Weber number and shock Mach number 14. Many tests were conducted between Mach 1.1 and 1.3 but later tests followed a switch to a dual depressurization procedure with an aluminum foil diaphragm which allowed for tests at higher Mach numbers. Mach number itself had no independent effect on the breakup regime. However, observed breakup modes tended to generally track with Gelfand's classifications. There were, however, a few cases of bag-and-stamen breakup at Weber numbers that would be expected to yield a bag breakup rather than a bag-and-stamen breakup. There was additionally one case at a Weber number above 60 where no breakup was observed. One possible explanation could stem from the fact that these tests were conducted by natural bursts rather than controlled electrical bursts. Since the diaphragm does not cleanly rupture under a natural burst, there is a risk that the flow in these cases was not uniform, and some fundamental assumptions did not hold. These cases will need to be investigated in more detail, however, before definite conclusions can be drawn.

VI. Conclusions

Atmospheric ice crystal aggregates observed in high-altitude clouds cause severe damage to hypersonic vehicles, which include satellites, re-entry vehicles, missiles, and jet aircraft. Despite this known hazard, experimental techniques allowing the study of the behavior of ice crystals in shockwaves are lacking, which inhibits any predictions for damage potential and airframe protection designs. Moreover, important properties of ice aggregates, such as bonding strength and thermodynamic conditions that promote their formation, remain under-explored. In this paper, the ability to generate atmosphericallyrelevant ice crystals and ice crystal aggregates is demonstrated in an acoustic levitator with two

temperature control mechanisms: a ScienTemp chest freezer, and a cryo-beaker. Inside a chest freezer, the acoustic levitator successfully generates ice crystals in the size ranges 500-600 μm, which matches the sizes of the chain-like ice crystal aggregates in recent flight campaigns such as those shown in Figure 4. Aggregation was also demonstrated in the chest freezer. The cryo-beaker setup shows that ice crystals are possible to generate external to the chest freezer. The setup achieves different ice crystal shapes generated from suspended water droplets. This approach successfully demonstrates different freezing mechanisms and indicates the possibility of incorporating it into the P3IST with further design modifications. The low temperature-DBET system traps atmospherically relevant microdroplets and can be reduced to -5.4°C. This setup is a new addition to hypersonic ground testing because it can freeze water droplets to produce ice crystals with known sizes and shapes and keep them in place to be introduced into high-speed flow facilities, such as the P3IST. The P3IST system is modified to demonstrate the breakup of water droplets with diameters approximately equal to 200 μm. Bag bursting is observed in the microdroplets after passing through the shockwave, as showin in Schlieren images. To observe ice crystal- shockwave interactions inside the shock-tube, precise timing synchronization among several components needs be done, such as the following: ice crystals falling time into the shock tube, the P3IST's diaphragm bursting time delay after entering the command in the operating software, and time calculation for the shockwave to reach the interaction point in a defined Mach speed . Therefore, this work also shows a plot that reports the time required for a shockwave to reach the first pressure sensor inside the shockwave at various Mach speeds. These key advancements in microparticle levitation instruments with low temperature control and modification of a shock tube to be able to introduce microdroplets and ice crystals will ultimately lead to a better understanding of the interaction between atmospherically realistic ice crystals and shockwaves.

Acknowledgments

The work conducted at the laboratory at UND and the facilities at Purdue was supported by the U.S. Department of Defense through the U.S. Office of Naval Research grant N00014-23-1-2269 (Program Officer: Eric Marineau). The use of OSCRE was supported by the National Science Foundation (NSF) under AGS #2233181.

We would like to thank Josefina Hajek-Herrera and Dr. Ryan Davis for their technical support with the DBET. Our gratitude also extends to Martin Schnaiter and Emma Järvinen for allowing us to use the PHIPS instrument during the CapeEx19 field project.

Additionally, we acknowledge Carson Lay and Mark Noftz for their valuable training on the shock tube and electrical burst system. Special thanks go to Terry Zhou for his invaluable advice and assistance with our optics setup, as well as Emma Nicotra for her help in configuring our trigger system for capturing high-speed video.

References

[1] Saunders, C. P. R., and Wahab, N. M. A., "The Influence of Electric Fields on the Aggregation of Ice Crystals," *Journal of the Meteorological Society of Japan. Ser. II*, Vol. 53, No. 2, 1975, pp. 121–126. https://doi.org/10.2151/jmsj1965.53.2_121, URL https://www.jstage.jst.go.jp/article/jmsj1965/53/2/53_2_121/_article.

[2] Liou, K.-N., "Transfer of solar irradiance through cirrus cloud layers," *Journal of Geophysical Research (1896-1977)*, Vol. 78, No. 9, 1973, pp. 1409–1418. https://doi.org/10.1029/JC078i009p01409, URL https://onlinelibrary.wiley.com/doi/abs/10.1029/JC078i009p01409, _eprint: https://onlinelibrary.wiley.com/doi/pdf/10.1029/JC078i009p01409.

[3] Murray, D. P., "A Study of Ice Particle Motion through a Shock Wave," Ph.D. thesis, Imperial College of London, 2010. URL http://spiral.imperial.ac.uk/handle/10044/1/6211, accepted: 2011-02-02T10:59:21Z Publisher: Imperial College London.

[4] Meng, H. C., and Ludema, K. C., "Wear models and predictive equations: their form and content," *Wear*, Vol. 181-183, 1995, pp. 443–457. https://doi.org/10.1016/0043-1648(95)90158-2, URL https://www.sciencedirect.com/science/article/pii/0043164895901582.

[5] Waldman, G. D., and Reinecke, W. G., "Particle trajectories, heating, and breakup in hypersonic shock layers," *AIAA Journal*, Vol. 9, No. 6, 1971, pp. 1040–1048. https://doi.org/10.2514/3.6328, URL https://arc.aiaa.org/doi/10.2514/3.6328.

[6] Lin, T. C., and Thyson, N. A., "Ice-crystal/shock-layer interaction in hypersonic flight," *AIAA Journal*, Vol. 15, No. 10, 1977, pp. 1511–1514. https://doi.org/10.2514/3.7446, URL https://arc.aiaa.org/doi/10.2514/3.7446.

[7] Nairy, C., "Observations Of Chain Aggregates In Florida Cirrus Cloud Anvils On 3 August 2019 During CAPEEX19," Ph.D. thesis, Jan. 2022. URL https://commons.und.edu/theses/4363.

[8] Abdelmonem, A., Schnaiter, M., Amsler, P., Hesse, E., Meyer, J., and Leisner, T., "First correlated measurements of the shape and light scattering properties of cloud particles using the new Particle Habit Imaging and Polar Scattering (PHIPS) probe," *Atmospheric Measurement Techniques*, Vol. 4, No. 10, 2011, pp. 2125–2142. https://doi.org/10.5194/amt-4-2125-2011, URL https://amt.copernicus.org/articles/4/2125/2011/, publisher: Copernicus GmbH.

[9] Nairy, C., Delene, D. J., Detwiler, A. G., Schmidt, J., Harasti, P., Schnaiter, M., Järvinen, E., and Walker, T., "Ice Crystal Chain Aggregates in Florida Cirrus Cloud Anvils - 3 August 2019 Case Study." *Journal of Geophysical Research: Atmospheres*, 2024. https://doi.org/InReview.

[10] Marzo, A., Barnes, A., and Drinkwater, B. W., "TinyLev: A multi-emitter single-axis acoustic levitator," *Review of Scientific Instruments*, Vol. 88, No. 8, 2017, p. 085105. https://doi.org/10.1063/1.4989995, URL https://pubs.aip.org/rsi/article/88/8/085105/962938/TinyLev-A-multi-emitter-single-axis-acoustic.

[11] Niemand, M., Möhler, O., Vogel, B., Vogel, H., Hoose, C., Connolly, P., Klein, H., Bingemer, H., DeMott, P., Skrotzki, J., and Leisner, T., "A Particle-Surface-Area-Based Parameterization of Immersion Freezing on Desert Dust Particles," 2012. https://doi.org/10.1175/JAS-D-11-0249.1, URL https://journals.ametsoc.org/view/journals/atsc/69/10/jas-d-11-0249.1.xml, section: Journal of the Atmospheric Sciences.

[12] Welti, A., Lüönd, F., Kanji, Z. A., Stetzer, O., and Lohmann, U., "Time dependence of immersion freezing: an experimental study on size selected kaolinite particles," *Atmospheric Chemistry and Physics*, Vol. 12, No. 20, 2012, pp. 9893–9907. https://doi.org/10.5194/acp-12-9893-2012, URL https://acp.copernicus.org/articles/12/9893/2012/, publisher: Copernicus GmbH.

[13] Hiranuma, N., Augustin-Bauditz, S., Bingemer, H., Budke, C., Curtius, J., Danielczok, A., Diehl, K., Dreischmeier, K., Ebert, M., Frank, F., Hoffmann, N., Kandler, K., Kiselev, A., Koop, T., Leisner, T., Möhler, O., Nillius, B., Peckhaus, A., Rose, D., Weinbruch, S., Wex, H., Boose, Y., DeMott, P. J., Hader, J. D., Hill, T. C. J., Kanji, Z. A., Kulkarni, G., Levin, E. J. T., McCluskey, C. S., Murakami, M., Murray, B. J., Niedermeier, D., Petters, M. D., O'Sullivan, D., Saito, A., Schill, G. P., Tajiri, T., Tolbert, M. A., Welti, A., Whale, T. F., Wright, T. P., and Yamashita, K., "A comprehensive laboratory study on the immersion freezing behavior of illite NX particles: a comparison of 17 ice nucleation measurement techniques," *Atmospheric Chemistry and Physics*, Vol. 15, No. 5, 2015, pp. 2489–2518. https://doi.org/10.5194/acp-15-2489-2015, URL https://acp.copernicus.org/articles/15/2489/2015/acp-15-2489-2015.html, publisher: Copernicus GmbH.

[14] Nagare, B., Marcolli, C., Welti, A., Stetzer, O., and Lohmann, U., "Comparing contact and immersion freezing from continuous flow diffusion chambers," *Atmospheric Chemistry and Physics*, Vol. 16, No. 14, 2016, pp. 8899–8914. https://doi.org/10.5194/acp-16-8899-2016, URL https://acp.copernicus.org/articles/16/8899/2016/, publisher: Copernicus GmbH.

[15] Hoffmann, N., Duft, D., Kiselev, A., and Leisner, T., "Contact freezing efficiency of mineral dust aerosols studied in an electrodynamic balance: quantitative size and temperature dependence for illite particles," *Faraday Discussions*, Vol. 165, No. 0, 2013, pp. 383–390. https://doi.org/10.1039/C3FD00033H, URL https://pubs.rsc.org/en/content/articlelanding/2013/fd/c3fd00033h, publisher: The Royal Society of Chemistry.

[16] DeMott, P. J., Prenni, A. J., McMeeking, G. R., Sullivan, R. C., Petters, M. D., Tobo, Y., Niemand, M., Möhler, O., Snider, J. R., Wang, Z., and Kreidenweis, S. M., "Integrating laboratory and field data to quantify the immersion freezing ice nucleation activity of mineral dust particles," *Atmospheric Chemistry and Physics*, Vol. 15, No. 1, 2015, pp. 393–409. https://doi.org/10.5194/acp-15-393-2015, URL https://acp.copernicus.org/articles/15/393/2015/, publisher: Copernicus GmbH.

[17] Kennedy, A., Scott, A., Loeb, N., Sczepanski, A., Lucke, K., Marquis, J., and Waugh, S., "Bringing Microphysics to the Masses: The Blowing Snow Observations at the University of North Dakota: Education through Research (BLOWN-UNDER) Campaign," 2022. https://doi.org/10.1175/BAMS-D-20-0199.1, URL https://journals.ametsoc.org/view/journals/bams/103/1/BAMS-D-20-0199.1.xml, section: Bulletin of the American Meteorological Society.

[18] "MATLAB Image Processing and Computer Vission," , 2024.

[19] Ardon-Dryer, K., and Levin, Z., "Ground-based measurements of immersion freezing in the eastern Mediterranean," *Atmospheric Chemistry and Physics*, Vol. 14, No. 10, 2014. https://doi.org/10.5194/acp-14-5217-2014, URL https://doi.org/10.5194/acp-14-5217-2014.

[20] López, M. L., and Ávila, E. E., "Measurements of natural deposition ice nuclei in Córdoba, Argentina," , 2012. https://doi.org/10.5194/acpd-12-31699-2012, URL https://doi.org/10.5194/acpd-12-31699-2012.

[21] Fornea, A. P., Brooks, S. D., Dooley, J. B., and Saha, A., "Heterogeneous freezing of ice on atmospheric aerosols containing ash, soot, and soil," *Journal of Geophysical Research: Atmospheres*, Vol. 114, No. D13, 2009. https://doi.org/10.1029/2009jd011958, URL https://doi.org/10.1029/2009jd011958.

[22] Lohmann, U., and Diehl, K., "Sensitivity Studies of the Importance of Dust Ice Nuclei for the Indirect Aerosol Effect on Stratiform Mixed-Phase Clouds," *Journal of the Atmospheric Sciences*, Vol. 63, No. 3, 2006. https://doi.org/10.1175/jas3662.1, URL https://doi.org/10.1175/jas3662.1.

[23] McElligott, A., Guerra, A., Wood, M. J., Rey, A. D., Kietzig, A.-M., and Servio, P., "TinyLev acoustically levitated water: Direct observation of collective, inter-droplet effects through morphological and thermal analysis of multiple droplets," *Journal of Colloid and Interface Science*, Vol. 619, 2022, pp. 84–95. https://doi.org/10.1016/j.jcis.2022.03.082, URL https://www.sciencedirect.com/science/article/pii/S0021979722004647.

[24] Birdsall, A. W., Krieger, U. K., and Keutsch, F. N., "Electrodynamic balance-mass spectrometry of single particles as a new platform for atmospheric chemistry research," *Atmos. Meas. Tech*, Vol. 11, 2018, pp. 33–47. https://doi.org/10.5194/amt-11-33-2018, URL https://doi.org/10.5194/amt-11-33-2018.

[25] Choczynski, J. M., Kaur Kohli, R., Sheldon, C. S., Price, C. L., and Davies, J. F., "A dual-droplet approach for measuring the hygroscopicity of aqueous aerosol," *Atmospheric Measurement Techniques*, Vol. 14, No. 7, 2021, pp. 5001–5013. https://doi.org/10.5194/amt-14-5001-2021.

[26] Davies, J. F., Haddrell, A. E., and Reid, J. P., "Time-resolved measurements of the evaporation of volatile components from single aerosol droplets," *Aerosol Science and Technology*, Vol. 46, No. 6, 2012, pp. 666–677. https://doi.org/10.1080/02786826.2011.652750.

[27] Haddrell, A. E., Davies, J. F., Yabushita, A., and Reid, J. P., "Accounting for Changes in Particle Charge, Dry Mass and Composition Occurring During Studies of Single Levitated Particles," *Journal of Physical Chemistry A*, Vol. 116, 2012, pp. 9941–9953. https://doi.org/10.1021/jp304920x, URL https://pubs.acs.org/sharingguidelines.

[28] Hart, M. B., Sivaprakasam, V., Eversole, J. D., Johnson, L. J., and Czege, J., "Optical measurements from single levitated particles using a linear electrodynamic quadrupole trap," *Applied Optics*, Vol. 54, No. 31, 2015, p. F174. https://doi.org/10.1364/ao.54.00f174.

[29] Petters, S. S., Hilditch, T. G., Tomaz, S., Miles, R. E., Reid, J. P., and Turpin, B. J., "Volatility Change during Droplet Evaporation of Pyruvic Acid," *ACS Earth and Space Chemistry*, Vol. 4, No. 5, 2020, pp. 741–749. https://doi.org/10.1021/acsearthspacechem.0c00044.

[30] Steimer, S. S., Krieger, U. K., Te, Y.-F., Lienhard, D. M., Huisman, A. J., Luo, B. P., Ammann, M., and Peter, T., "Electrodynamic balance measurements of thermodynamic, kinetic, and optical aerosol properties inaccessible to bulk methods," *Atmos. Meas. Tech*, Vol. 8, 2015, pp. 2397–2408. https://doi.org/10.5194/amt-8-2397-2015, URL www.atmos-meas-tech.net/8/2397/2015/.

[31] Willis, M. D., Rovelli, G., and Wilson, K. R., "Combining Mass Spectrometry of Picoliter Samples with a Multicompartment Electrodynamic Trap for Probing the Chemistry of Droplet Arrays," *Anal. Chem*, Vol. 16, 2020, p. 43. https://doi.org/10.1021/acs.analchem.0c02343, URL https://dx.doi.org/10.1021/acs.analchem.0c02343, publisher: UTC.

[32] Jacobs, M. I., Davis, R. D., Rapf, R. J., and Wilson, K. R., "Studying Chemistry in Micro-compartments by Separating Droplet Generation from Ionization," *American Society for Mass Spectrometry*, Vol. 30, 2019, pp. 339–343. https://doi.org/10.1007/s13361-018-2091-y.

[33] Jacobs, M. I., Davies, J. F., Lee, L., Davis, R. D., Houle, F., and Wilson, K. R., "Exploring Chemistry in Microcompartments Using Guided Droplet Collisions in a Branched Quadrupole Trap Coupled to a Single Droplet, Paper Spray Mass Spectrometer," *Analytical Chemistry*, Vol. 89, No. 22, 2017, pp. 12511–12519. https://doi.org/10.1021/acs.analchem.7b03704.

[34] Richards, D. S., Trobaugh, K. L., Hajek-Herrera, J., and Davis, R. D., "Dual-Balance Electrodynamic Trap as a Microanalytical Tool for Identifying Gel Transitions and Viscous Properties of Levitated Aerosol Particles," *Analytical Chemistry*, Vol. 92, No. 4, 2020, pp. 3086–3094. https://doi.org/10.1021/acs.analchem.9b04487, URL https://doi.org/10.1021/acs.analchem.9b04487, publisher: American Chemical Society.

[35] French, J. R., Friedrich, K., Tessendorf, S. A., Rauber, R. M., Geerts, B., Rasmussen, R. M., Xue, L., Kunkel, M. L., and Blestrud, D. R., "Precipitation formation from orographic cloud seeding," Vol. 117, No. 6, 2018, pp. 1168–1173. https://doi.org/10.1073/pnas.1716995115, URL www.pnas.org/cgi/doi/10.1073/pnas.1716995115.

[36] Vonnegut, B., "The Nucleation of Ice Formation by Silver Iodide," *Journal of Applied Physics*, Vol. 18, No. 7, 1947, pp. 593–595. https://doi.org/https://doi.org/10.1063/1.1697813.

[37] Soni, A., and Patey, G. N., "Ice Nucleation by the Primary Prism Face of Silver Iodide," *The Journal of Physical Chemistry C*, Vol. 126, No. 15, 2022, pp. 6716–6723. https://doi.org/10.1021/acs.jpcc.1c10227, URL https://doi.org/10.1021/acs.jpcc.1c10227, publisher: American Chemical Society.

[38] Ojo, V., Osmani, I., Roadifer, L., Berner, M., Miller, Z., Newcomer, C., Hajek-Herrera, J., Davis, R., Zhang, Z., Gagan, S., Zhang, Y., and Chelmo, H. B., "Low-Temperature Dual Balance Electrodynamic Trap (LT-DBET) for Single Microparticle Aerosol Studies," *Aerosol Science and Technology*, 2024. https://doi.org/InReview.

[39] Wason, and Mark, "Calibration of High-Frequency Pressure Sensors Using Low-Pressure Shock Waves," Ph.D. thesis, Purdue University, West Lafayette, Indiana, 2019.

[40] Berridge, D. C., "Generating Low-Pressure Shock Waves for Calibrating High-Frequency Pressure Sensors," Ph.D. thesis, Purdue University, West Lafayette, Indiana, 2015.

[41] Sharma, S., Singh, A. P., Rao, S. S., Kumar, A., and Basu, S., "Shock induced aerobreakup of a droplet," *Journal of Fluid Mechanics*, Vol. 929, 2021, p. A27. https://doi.org/10.1017/jfm.2021.860, URL https://www.cambridge.org/core/journals/journal-of-fluid-mechanics/article/shock-induced-aerobreakup-of-a-droplet/8E93F9A8CD57CF53A2BC7DD366DF7364.

[42] Poplavski, S. V., Minakov, A. V., Shebeleva, A. A., and Boyko, V. M., "On the interaction of water droplet with a shock wave: Experiment and numerical simulation," *International Journal of Multiphase Flow*, Vol. 127, 2020, p. 103273. https://doi.org/10.1016/j.ijmultiphaseflow.2020.103273, URL https://www.sciencedirect.com/science/article/pii/S0301932219303817.